



Sensitivity of superconducting states to the impurity location in layered materials

Bastian Zinkl ¹ and Aline Ramires ²

¹*Institute for Theoretical Physics, ETH Zurich, CH-8093 Zurich, Switzerland*

²*Condensed Matter Theory Group, Paul Scherrer Institute, CH-5232 Villigen PSI, Switzerland*



(Received 2 February 2022; revised 2 July 2022; accepted 12 July 2022; published 20 July 2022)

The family of multilayered superconductors derived from doped topological insulators in the family of Bi_2Se_3 has been found to be unusually robust against nonmagnetic disorder. Recent experimental studies have highlighted the fact that the location of impurities could play a critical role in this puzzling robustness. Here we investigate the effects of four different types of impurities, on-site, interstitial, intercalated, and polar, on the superconducting critical temperature. We find that different components of the scattering potential are active depending on the impurity configuration and choice of orbitals for the effective low-energy description of the normal state. For the specific case of Bi_2Se_3 -based superconductors, we find that only the symmetric share of impurity configurations contribute to scattering, such that polar impurities are completely inactive. We also find that a more dominant mass-imbalance term in the normal-state Hamiltonian can make the superconducting state more robust to intercalated impurities, in contrast to the case of on-site or interstitial impurities.

DOI: [10.1103/PhysRevB.106.014515](https://doi.org/10.1103/PhysRevB.106.014515)

I. INTRODUCTION

The effects of impurities in simple superconductors are well understood in terms of elementary symmetry arguments, elegantly summarized in what is known as Anderson's theorem [1,2]. In fully gapped conventional superconductors, Cooper pairs are formed between electrons related by time-reversal symmetry. As a consequence, impurities have a detrimental effect on superconductivity only if they break this key symmetry, namely, if the impurities are magnetic. For unconventional nodal superconductors both magnetic and nonmagnetic disorder have a negative effect on the critical temperature [3,4]. The sensitivity of superconductors to nonmagnetic disorder has therefore been taken as a strong indication of the unconventional nature of the order parameter, as observed in UPt_3 [5], Sr_2RuO_4 [6], and in the cuprates [7], to name a few.

In contrast, the effects of impurities in complex superconductors have only recently started to attract attention, mostly motivated by the phenomenology of iron-based superconductors [8–10]. Complex superconductors are characterized by multiple Fermi surfaces, or by single Fermi surfaces emerging from a combination of multiple internal degrees of freedom. In this context, one result that goes beyond the prediction of Anderson's theorem concerns fully gapped superconductors in multiband systems. A two-band system with full gaps of opposite signs is known to be sensitive to nonmagnetic disorder [8–10]. Naturally, the extra sensitivity to disorder of such fully gapped systems is not a desirable feature to explore potential applications of these materials.

Intriguingly, the traditional picture has recently been challenged by the observation of unconventional superconductors that are unusually robust against nonmagnetic doping. For instance, the superconductor $\text{Cu}_x(\text{PbSe})_5(\text{Bi}_2\text{Se}_3)_6$ [11],

showing nematic properties and a nodal gap structure [12], survives scattering rates much larger than anticipated by Anderson's theorem [13]. Other materials in the same family, $\text{Cu}_x\text{Bi}_2\text{Se}_3$ [14–16] and $\text{Nb}_x\text{Bi}_2\text{Se}_3$ [17–19], also display unusual robustness against nonmagnetic disorder. In-doped SnTe remarkably shows a larger critical temperature for samples with high residual resistivity [20]. Irradiated PdTe_2 also shows robustness against nonmagnetic disorder, with its critical temperature suppressed at a rate that is about sixteen times slower than predicted by standard estimations [21].

The first theories developed to address this unusual robustness were based on the presence of strong spin-orbit coupling (SOC) [22,23]. Later, it became clear that for complex superconductors (with extra internal degrees of freedom such as orbitals or sublattices), the concept of superconducting fitness allows for a generalization of Anderson's theorem, providing a universal framework and explanation for the unusual robustness of unconventional superconducting states [13,21,24]. Specific results for Cu-doped Bi_2Se_3 report that the robustness of the superconducting state depends not only on the superconducting order parameter, but on details of the electronic structure in the normal state [25]. Recently, this understanding was corroborated by a more complete analysis of the sensitivity of pairing states to various scattering potentials in two-orbital systems [24,26,27].

Here we focus on superconductors derived from Bi_2Se_3 . Common among these materials is the basic crystallographic unit consisting of quintuple layers (Se-Bi-Se''-Bi'-Se') [28], as schematically depicted in Fig. 1. Superconductivity emerges in these systems only after doping, which intrinsically also introduces disorder. The location of impurities within these layers has attracted some interest, since evidence has accumulated that their distribution, and not just the electron donation, plays a decisive role for the formation of

unconventional superconductivity [29]. Density-functional theory calculations suggest that the most energetically favorable location for Cu [30] and Sr [31] dopants should be between the quintuple layers, i.e., in the van der Waals (vdW) gap. X-ray diffraction experiments seem to support this suggestion, since an expansion of the c axis has been observed in both $\text{Cu}_x\text{Bi}_2\text{Se}_3$ [32–34] and $\text{Sr}_x\text{Bi}_2\text{Se}_3$ [35,36]. However, dopants in the vdW gap have not been directly detected so far, either with neutron-scattering experiments in the case of $\text{Cu}_x\text{Bi}_2\text{Se}_3$ [34] or with transmission electron microscopy in the case of $\text{Sr}_x\text{Bi}_2\text{Se}_3$ [31]. In the latter compound the vertical position of the impurities has only recently been determined using normal-incidence x-ray standing wave measurements [29]. It was found that the dopants lie close to the Se and Se' sites with a small vertical displacement toward the center of the quintuple layer, hence not in the vdW gap. Lastly, for Nb-doped Bi_2Se_3 it was initially assumed that superconductivity is induced by impurities located in the vdW layers [37]. However, recent observations rather suggest that its origin lies in the $(\text{BiSe})_{1.10}\text{NbSe}_2$ misfit phase, which is characterized by structural deformations [38].

Motivated by these observations, we investigate in detail how the location of impurities influence the renormalization of the critical temperature in layered superconductors. Using Bi_2Se_3 as our example, we derive the scattering matrices for four different scenarios: substitutional (on-site), interstitial (in between two sites), intercalated (in the vdW gap), and polar defects, as illustrated in Fig. 2. We start with an effective microscopic model for the electronic states in the quintuple layers and analyze the effects of impurities in case different pairs of orbitals dominate the effective low-energy electronic structure. Here we are guided by the concept of superconducting fitness and the generalized Anderson's theorem to discuss the robustness of superconducting states in multiple scenarios.

This paper is organized as follows. In Sec. II we review the microscopic description of the electronic structure of materials in the family of doped Bi_2Se_3 and the possible s -wave superconducting states. In Sec. III after modeling different impurity configurations in the layer basis, we discuss how these manifest in effective two-orbital models. In Sec. IV we then evaluate the effective scattering rates for different impurity distributions and effective model scenarios. Finally, in Sec. V we summarize our findings and how these can help us understand the unusual robustness of superconducting states in layered materials.

II. EFFECTIVE MICROSCOPIC DESCRIPTION

In this section, we introduce and discuss the microscopic structure of the normal-state Hamiltonian and the superconducting order parameters.

A. Normal state

Motivated by the phenomenology of Bi_2Se_3 -based superconductors, we start modeling the electronic structure in the quintuple layer of these materials. First-principles calculations suggest that the main orbitals contributing to the low-energy electronic structure of Bi_2Se_3 stem from p_z orbitals located at the four outermost layers (Se-Bi-Bi'-Se'),

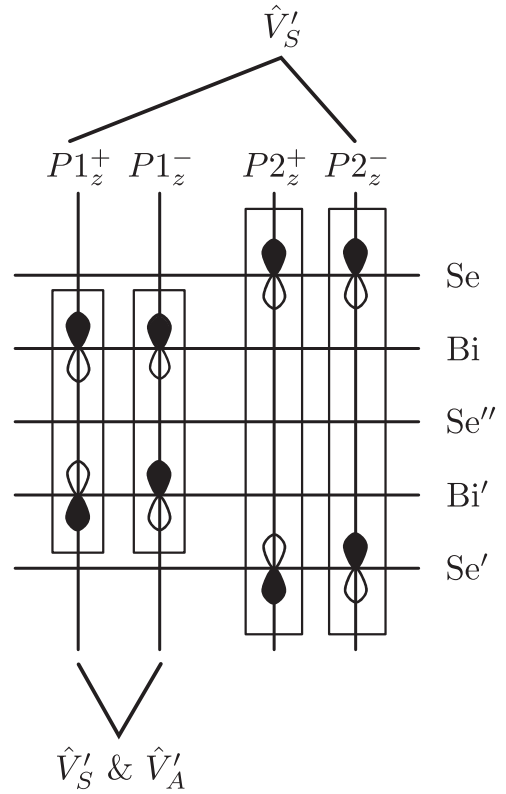


FIG. 1. Side view of the quintuple layer unit cell of Bi_2Se_3 . We illustrate the $P1_z^\alpha$ orbitals as symmetric ($\alpha = +$) or antisymmetric ($\alpha = -$) combinations of the p_z orbitals in each layer. We also highlight which scattering matrices remain relevant, if two specific states are chosen as the low-energy basis. As examples, we consider the combinations $\{P1_z^+, P2_z^-\}$ (top) and $\{P1_z^+, P1_z^-\}$ (bottom). More details on the matrix structures are given in Table IV.

here labeled as $|S_z\rangle$, $|B_z\rangle$, $|B'_z\rangle$, $|S'_z\rangle$, respectively [28]. It is convenient to combine these in bonding and antibonding configurations,

$$|P1_z^\pm\rangle = \frac{1}{\sqrt{2}}(|B_z\rangle \mp |B'_z\rangle), \quad (1)$$

$$|P2_z^\pm\rangle = \frac{1}{\sqrt{2}}(|S_z\rangle \mp |S'_z\rangle), \quad (2)$$

which are schematically indicated in Fig. 1. Note that the upper index corresponds to the parity of the state.

The states written down in Eqs. (1) and (2) constitute what we call the “orbital” basis, denoted by $\{P1_z^+, P1_z^-, P2_z^+, P2_z^-\}$. In the “layer” basis $\{\text{Se}, \text{Bi}, \text{Bi}', \text{Se}'\}$ they take the form

$$|P1_z^\pm\rangle = \frac{1}{\sqrt{2}} \begin{pmatrix} 0 \\ 1 \\ \mp 1 \\ 0 \end{pmatrix}, \quad |P2_z^\pm\rangle = \frac{1}{\sqrt{2}} \begin{pmatrix} 1 \\ 0 \\ 0 \\ \mp 1 \end{pmatrix}. \quad (3)$$

TABLE I. Parametrization of the normal-state Hamiltonian [Eq. (5)] for materials in the family of Bi_2Se_3 assuming orbitals with OP. For each pair of indexes (a, b) corresponding to the basis matrices $\hat{\tau}_a \otimes \hat{\sigma}_b$, the table highlights the irreducible representations (Irrep) and the physical process that originates them. The last column gives the expansion of the form factors $h_{ab}(\mathbf{k})$ for small momentum.

(a, b)	Irrep	Process	$h_{ab}(\mathbf{k})$
(0,0)	A_{1g}	Intraorbital hopping	$C_0 + C_1 k_z^2 + C_2(k_x^2 + k_y^2)$
(3,0)	A_{1g}	Intraorbital hopping	$M_0 + M_1 k_z^2 + M_2(k_x^2 + k_y^2)$
(1,3)	A_{1u}	SOC	$R_1 k_x(k_x^2 - 3k_y^2)$
(2,0)	A_{2u}	Interorbital hopping	$B_0 k_z$
(1,1)	E_u	SOC	$-A_0 k_y$
(1,2)	E_u	SOC	$A_0 k_x$

The unitary transformation matrix corresponding to this basis change is

$$\hat{U} = \frac{1}{\sqrt{2}} \begin{pmatrix} 0 & 0 & 1 & 1 \\ 1 & 1 & 0 & 0 \\ -1 & 1 & 0 & 0 \\ 0 & 0 & -1 & 1 \end{pmatrix}, \quad (4)$$

which will be important in Sec. III, where we analyze the structure of different impurity configurations in different reduced orbital bases.

For Bi_2Se_3 -based materials, it is clear from first principles that only two of these orbitals contribute to the Fermi surface. In particular, it is suggested that these orbitals are $\{P1_z^+, P2_z^-\}$ [28]. More generally, we can think of any pair of orbitals effectively contributing to the Fermi surface. There are three fundamentally distinct scenarios: (i) two orbitals with opposite parity (OP) coming from different types of atoms (this would be the case of Bi_2Se_3 -based materials just mentioned, but also $\{P2_z^+, P1_z^-\}$); (ii) two orbitals with OP coming from the same type of atoms ($\{P1_z^+, P1_z^-\}$ or $\{P2_z^+, P2_z^-\}$); (iii) two orbitals with equal parity (EP), necessarily associated with different atoms ($\{P1_z^+, P2_z^+\}$ or $\{P1_z^-, P2_z^-\}$).

For all these cases the low-energy Hamiltonian of the system can be parametrized as

$$\hat{H}(\mathbf{k}) = \sum_{a,b} h_{ab}(\mathbf{k})(\hat{\tau}_a \otimes \hat{\sigma}_b), \quad (5)$$

where $\hat{\tau}_a$ and $\hat{\sigma}_b$, with $\{a, b\} \in \{0, 1, 2, 3\}$, are Pauli matrices encoding the orbital and spin degrees of freedom, respectively. The explicit momentum dependence of the $h_{ab}(\mathbf{k})$ terms in the normal-state Hamiltonian depends on the point group symmetry of the system. The point group D_{3d} can be generated by the following symmetry operations: $P = \hat{\tau}_a \otimes \hat{\sigma}_0$, parity; $C_{3z} = \hat{\tau}_0 \otimes e^{i\frac{2\pi}{3}\hat{\sigma}_3}$, a rotation by $2\pi/3$ around the z axis; and $C_{2x} = \hat{\tau}_a \otimes e^{i\frac{\pi}{2}\hat{\sigma}_1}$, a rotation by π along the x axis (with $a = 0$ for EP and $a = 3$ for OP orbitals). For the OP scenario, the symmetry-allowed terms in the Hamiltonian are the ones summarized in Table I. Analogously, for the EP scenario, we obtain the terms listed in Table II.

TABLE II. Parametrization of the normal-state Hamiltonian [Eq. (5)] for the EP scenario. Same description as in Table I.

(a, b)	Irrep	Process	$h_{ab}(\mathbf{k})$
(0,0)	A_{1g}	Intraorbital hopping	$C'_0 + C'_1 k_z^2 + C'_2(k_x^2 + k_y^2)$
(3,0)	A_{1g}	Intraorbital hopping	$M'_0 + M'_1 k_z^2 + M'_2(k_x^2 + k_y^2)$
(1,0)	A_{1g}	Interorbital hopping	$N'_0 + N'_1 k_z^2 + N'_2(k_x^2 + k_y^2)$
(2,3)	A_{2g}	SOC	$R'_1 k_x k_z(k_x^2 - 3k_y^2)$
(2,1)	E_g	SOC	$-A'_0 k_y k_z$
(2,2)	E_g	SOC	$A'_0 k_x k_z$

B. Superconducting state

The order parameter of the superconducting state can be written as

$$\hat{\Delta}(\mathbf{k}) = \sum_{a,b} d_{ab}(\mathbf{k})[\hat{\tau}_a \otimes \hat{\sigma}_b(i\hat{\sigma}_2)]. \quad (6)$$

From now on we implicitly assume that the order parameter is normalized, i.e., $\langle ||\hat{\Delta}(\mathbf{k})||^2 \rangle_{\text{FS}} = 1$, where $\langle \dots \rangle_{\text{FS}}$ denotes the average over the Fermi surface, and $||\hat{M}||^2 = \text{Tr}[\hat{M}\hat{M}^\dagger]/4$ is the Frobenius norm of the matrix \hat{M} . Fermionic antisymmetry requires $\hat{\Delta}(\mathbf{k}) = -\hat{\Delta}^T(-\mathbf{k})$, what means that even- \mathbf{k} (odd- \mathbf{k}) order parameters are necessarily accompanied by antisymmetric (symmetric) matrices. In the following, we restrict ourselves to \mathbf{k} -independent $d_{ab}(\mathbf{k})$, also referred to as s -wave superconducting states. Note, though, that once the problem is rewritten in the band basis and the superconducting gap is projected onto the Fermi surface, the order parameters in non-trivial irreducible representations generally develop nodes. See for example the discussion in Ref. [13].

This restriction reduces the space of order parameters to the six antisymmetric basis matrices listed in Table III. Note that they are labeled as $[a, b]$ (rectangular brackets are used to label the superconducting states, while round brackets label the terms in the normal-state Hamiltonian) and that they are independent of the choice of EP or OP orbitals contributing to the Fermi surface. However, as summarized in Table III, the parity of the orbitals influences the symmetry of the order parameter and its associated irreducible representation. Order parameters with a symmetry-enforced \mathbf{k} dependence in the

TABLE III. Momentum-independent superconducting order parameters for two-orbital models. We highlight here the spin and orbital characters as well as the irreducible representation of the respective gap matrix for the opposite-parity (OP) and equal-parity (EP) cases.

$[a, b]$	Spin	Orbital	Irrep (OP)	Irrep (EP)
[0,0]	Singlet	Symmetric	A_{1g}	A_{1g}
[3,0]	Singlet	Symmetric	A_{1g}	A_{1g}
[2,3]	Triplet	Antisymmetric	A_{1u}	A_{2g}
[1,0]	Singlet	Symmetric	A_{2u}	A_{1g}
[2,1]	Triplet	Antisymmetric	E_u	E_g
[2,2]	Triplet	Antisymmetric	E_u	E_g

orbital basis can also be analyzed within our framework, but the suppression of the superconducting critical temperature as a function of impurities is purely determined by the normal-state properties as the momentum average of the order parameter, and consequently the superconducting scattering rate, is zero. This is going to be discussed in detail in Sec. IV C.

C. The concept of superconducting fitness

The concept of superconducting fitness was originally introduced as a theoretical tool to concisely address the effects of external symmetry-breaking fields [39,40]. Later, the same concept was shown to be useful in the context of electronic structure engineering for the optimization of the superconducting critical temperature [41]. More recently, this concept was proved to be related to a variety of unusual properties and responses in unconventional superconductors: the presence of odd-frequency correlations [42]; anomalous Hall effect in chiral superconductors [43]; opening of high-energy gaps in nonunitary superconductors [44]; abnormal evolution of the critical temperature under strain [45]; the presence of gap nodes in superconductors associated with local pairing interactions [46]; photon-induced supercurrents in anapole superconductors [47]; and Bogoliubov Fermi surfaces in even-parity time-reversal symmetry-breaking superconductors [48].

Within the standard weak-coupling theories for superconductivity, if pairing happens between electrons in the same band (intra-band pairing), superconductivity is very robust and is established for an arbitrarily small attractive interaction through the formation of electron pairs with total zero momentum. If pairing happens between electrons in different bands (inter-band pairing), superconductivity is not so robust as a finite attractive interaction is necessary for the onset of superconductivity. Based on these basic ideas, below we present a heuristic discussion and introduction of the concept of superconducting fitness. Here we closely follow the discussion provided in Ref. [39].

In the presence of external symmetry-breaking fields or multiple orbitals or sublattices, the normal-state Hamiltonian $\hat{H}(\mathbf{k})$ is generally not diagonal in the microscopic basis. As the Hamiltonian is a Hermitian matrix, there is always a unitary transformation $\hat{U}(\mathbf{k})$ which diagonalizes it, or rotates it to the band basis: $\hat{H}_B(\mathbf{k}) = \hat{U}(\mathbf{k})\hat{H}(\mathbf{k})\hat{U}^\dagger(\mathbf{k})$ (the subscript B stands for the band basis). The gap matrix, by connecting particle and hole spaces, transforms in a slightly different manner: $\hat{\Delta}_B(\mathbf{k}) = \hat{U}(\mathbf{k})\hat{\Delta}(\mathbf{k})\hat{U}^T(-\mathbf{k})$. In the case of pure intra-band pairing $\hat{\Delta}_B(\mathbf{k})$ is block diagonal. A non-block-diagonal gap matrix is an indication of inter-band pairing.

To get some intuition on the origin of the concept of superconducting fitness, we consider the minimal multi-orbital problem consisting of two orbitals with an internal spin degree of freedom. In the presence of time-reversal and inversion symmetries, the eigenstates ϵ_a (a is the band label) of $\hat{H}_B(\mathbf{k})$ are doubly degenerate and as a consequence $\hat{H}_B(\mathbf{k})$ has a structure with 2×2 blocks proportional to the identity $\hat{\sigma}_0$ in the pseudospin sector. Concerning the gap matrix, an arbitrary gap structure has both intra-band, $\hat{\Delta}_a$, and inter-band, $\hat{\Delta}_{ab}$, components. Under these conditions, omitting the momentum

dependence we can write

$$\hat{H}_B = \begin{pmatrix} \epsilon_1 \hat{\sigma}_0 & 0 \\ 0 & \epsilon_2 \hat{\sigma}_0 \end{pmatrix}, \quad \hat{\Delta}_B = \begin{pmatrix} \hat{\Delta}_1 & \hat{\Delta}_{12} \\ \hat{\Delta}_{21} & \hat{\Delta}_2 \end{pmatrix}. \quad (7)$$

Note that these matrices do not commute for finite inter-band pairing, unless the artificial condition $\epsilon_1 = \epsilon_2$ is satisfied. On the other hand, in case $\hat{\Delta}_{ab}(\mathbf{k}) = 0$, $\hat{\Delta}_B(\mathbf{k})$ is block diagonal and commutes with the bare Hamiltonian $\hat{H}_B(\mathbf{k})$ in the band basis.

Taking the condition of pure intra-band pairing as the one leading to the most robust superconducting instability, we can then look at this condition in the microscopic basis. Using the unitary transformation introduced above and the fact that $\hat{H}_B(\mathbf{k})$ and $\hat{\Delta}_B(\mathbf{k})$ commute in case of pure intra-band pairing, we obtain

$$\hat{H}(\mathbf{k})\hat{\Delta}(\mathbf{k}) - \hat{\Delta}(\mathbf{k})\hat{H}^T(-\mathbf{k}) = 0. \quad (8)$$

If $\hat{H}(\mathbf{k})$ and $\hat{\Delta}(\mathbf{k})$ satisfy this condition, the system develops only intra-band pairing and consequently has the most robust superconducting instability. In case the identity above is not satisfied, we have a measure of the incompatibility between the superconducting state and the normal state, associated with the presence of inter-band pairing, which we label as the superconducting fitness matrix $\hat{F}_C(\mathbf{k})$,

$$\hat{F}_C(\mathbf{k}) = \hat{H}(\mathbf{k})\hat{\Delta}(\mathbf{k}) - \hat{\Delta}(\mathbf{k})\hat{H}^T(-\mathbf{k}). \quad (9)$$

This measure was also identified within the discussion of the compatibility or incompatibility of superconducting states regarding disorder, in the form of what is called the generalized Anderson's theorem [13]. In the original version of Anderson's theorem [1], the robustness of the superconducting state was argued based on symmetry aspects. If the impurities do not break the symmetry that connects the two states in the Cooper pair (for conventional superconductors this is inversion symmetry), then it is guaranteed that the order parameter is robust. In its generalized form, this information is encoded in the commutation relation between the impurity potential and the superconducting gap matrices. If these matrices commute, they are compatible in the sense that they can be diagonalized in the same basis and the superconducting state is then robust in the presence of impurities. If these matrices do not commute they are incompatible; impurities now scramble the states and are pair breaking. As a consequence of this incompatibility, the superconducting critical temperature is reduced.

Having clarified our microscopic model and the concept of superconducting fitness, we consider in the following different scattering potentials out of nonmagnetic impurities.

III. IMPURITY CONFIGURATIONS IN THE QUINTUPLE LAYER AND ORBITAL BASES

To unveil the effects of the impurity location in materials belonging to the family of Bi_2Se_3 , we distinguish between on-site (on), interstitial (is), intercalated (ic), and polar (po) configurations, which are illustrated in Fig. 2.

The scattering matrices written in the layer basis $\{\text{Se}, \text{Bi}, \text{Bi}', \text{Se}'\}$ have an entry on the diagonal, if the corresponding layer is affected by the impurity. For instance, the on-site

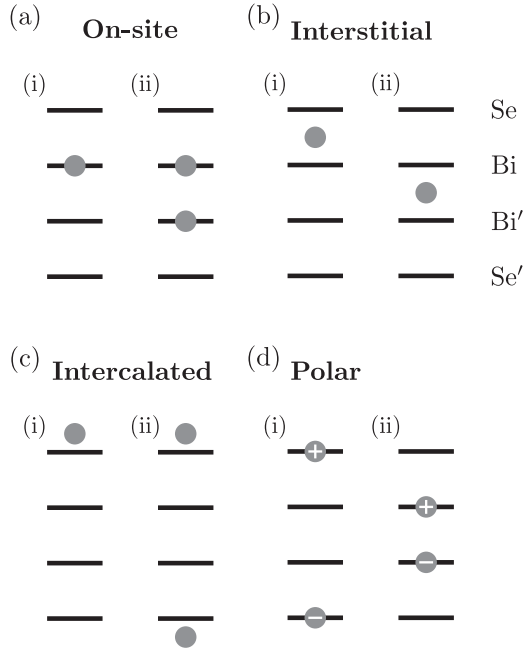


FIG. 2. Schematic illustration of (a) on-site, (b) interstitial, (c) intercalated, and (d) polar impurity configurations (marked as dark gray circles). In Eqs. (16) to (18) we show that the scattering potential can be always decomposed into a superposition of a symmetric and an antisymmetric impurity potential. The polar configuration consists of oppositely charged impurities in opposite layers, which leads to a fully antisymmetric potential [Eq. (19)].

configurations shown in Fig. 2(a) are given by

$$\hat{V}_{\text{on}}^{(i)} = \begin{pmatrix} 0 & 0 & 0 & 0 \\ 0 & V & 0 & 0 \\ 0 & 0 & 0 & 0 \\ 0 & 0 & 0 & 0 \end{pmatrix}, \quad \hat{V}_{\text{on}}^{(ii)} = \begin{pmatrix} 0 & 0 & 0 & 0 \\ 0 & 0 & 0 & 0 \\ 0 & 0 & V & 0 \\ 0 & 0 & 0 & 0 \end{pmatrix}, \quad (10)$$

where $V > 0$ denotes the impurity scattering strength, which we take to be the same for all impurities. If the impurities are located between the Bi and Se sites, as in Fig. 2(b), we call them interstitial and assume that their presence affects both neighboring layers, which leads to

$$\hat{V}_{\text{is}}^{(i)} = \begin{pmatrix} V & 0 & 0 & 0 \\ 0 & V & 0 & 0 \\ 0 & 0 & 0 & 0 \\ 0 & 0 & 0 & 0 \end{pmatrix}, \quad \hat{V}_{\text{is}}^{(ii)} = \begin{pmatrix} 0 & 0 & 0 & 0 \\ 0 & V & 0 & 0 \\ 0 & 0 & V & 0 \\ 0 & 0 & 0 & 0 \end{pmatrix}. \quad (11)$$

Correspondingly, we find for the intercalated scenario, depicted in Fig. 2(c),

$$\hat{V}_{\text{ic}}^{(i)} = \begin{pmatrix} V & 0 & 0 & 0 \\ 0 & 0 & 0 & 0 \\ 0 & 0 & 0 & 0 \\ 0 & 0 & 0 & 0 \end{pmatrix}, \quad \hat{V}_{\text{ic}}^{(ii)} = \begin{pmatrix} V & 0 & 0 & 0 \\ 0 & 0 & 0 & 0 \\ 0 & 0 & 0 & 0 \\ 0 & 0 & 0 & V \end{pmatrix}, \quad (12)$$

and for the polar case, exemplified in Fig. 2(d),

$$\hat{V}_{\text{po}}^{(i)} = \begin{pmatrix} V & 0 & 0 & 0 \\ 0 & 0 & 0 & 0 \\ 0 & 0 & 0 & 0 \\ 0 & 0 & 0 & -V \end{pmatrix}, \quad \hat{V}_{\text{po}}^{(ii)} = \begin{pmatrix} 0 & 0 & 0 & 0 \\ 0 & V & 0 & 0 \\ 0 & 0 & -V & 0 \\ 0 & 0 & 0 & 0 \end{pmatrix}. \quad (13)$$

There are two linearly independent symmetric (S) configurations, which are even under inversion. They take the form

$$\hat{V}_{\text{S},1} = \begin{pmatrix} V & 0 & 0 & 0 \\ 0 & 0 & 0 & 0 \\ 0 & 0 & 0 & 0 \\ 0 & 0 & 0 & V \end{pmatrix}, \quad \hat{V}_{\text{S},2} = \begin{pmatrix} 0 & 0 & 0 & 0 \\ 0 & V & 0 & 0 \\ 0 & 0 & V & 0 \\ 0 & 0 & 0 & 0 \end{pmatrix}. \quad (14)$$

The antisymmetric (A) counterparts are given by

$$\hat{V}_{\text{A},1} = \begin{pmatrix} V & 0 & 0 & 0 \\ 0 & 0 & 0 & 0 \\ 0 & 0 & 0 & 0 \\ 0 & 0 & 0 & -V \end{pmatrix}, \quad \hat{V}_{\text{A},2} = \begin{pmatrix} 0 & 0 & 0 & 0 \\ 0 & V & 0 & 0 \\ 0 & 0 & -V & 0 \\ 0 & 0 & 0 & 0 \end{pmatrix}. \quad (15)$$

Every impurity configuration can be split up into symmetric and antisymmetric parts using Eqs. (14) and (15). For example, the configurations introduced above can be rewritten as

$$\hat{V}_{\text{on}}^{(i)} = \frac{1}{2}(\hat{V}_{\text{S},2} + \hat{V}_{\text{A},2}), \quad \hat{V}_{\text{on}}^{(ii)} = \hat{V}_{\text{S},2}, \quad (16)$$

$$\hat{V}_{\text{is}}^{(i)} = \frac{1}{2}(\hat{V}_{\text{S},1} + \hat{V}_{\text{S},2} + \hat{V}_{\text{A},1} + \hat{V}_{\text{A},2}), \quad \hat{V}_{\text{is}}^{(ii)} = \hat{V}_{\text{S},2}, \quad (17)$$

$$\hat{V}_{\text{ic}}^{(i)} = \frac{1}{2}(\hat{V}_{\text{S},1} + \hat{V}_{\text{A},1}), \quad \hat{V}_{\text{ic}}^{(ii)} = \hat{V}_{\text{S},1}, \quad (18)$$

and

$$\hat{V}_{\text{po}}^{(i)} = \hat{V}_{\text{A},1}, \quad \hat{V}_{\text{po}}^{(ii)} = \hat{V}_{\text{A},2}. \quad (19)$$

Using this framework, we can decompose every possible impurity distribution for a single unit cell in terms of symmetric and antisymmetric scattering matrices. Assuming a system with N_{uc} unit cells, each with four layers, the maximum number of impurities is equal to $N_{\text{max}} = 4N_{uc}$, $3N_{uc}$, or $2N_{uc}$ for on-site, interstitial, or intercalated and polar configurations, respectively. For a fixed number of impurities it is a straightforward combinatorial problem to find all possible impurity configurations. To give a concrete example, we show all possible, on-site configurations for $N_{uc} = 1$ in Fig. 3. For a single impurity, $n = N/N_{\text{max}} = 1/4$, there are only asymmetric configurations. These can be decomposed into a sum of symmetric and antisymmetric potentials, which leads to a symmetric share $S(n) = 1/2$. The symmetric share increases with growing N until it reaches one for the completely filled unit cell ($n = 1$). By calculating the symmetric share numerically for all different configurations and for an arbitrary large number of sites we find that $S(n)$ quickly converges to a universal result, which is depicted by the solid lines in Fig. 4. The dashed lines represent the antisymmetric shares $A(n) = 1 - S(n)$. Note that for polar impurities, whose

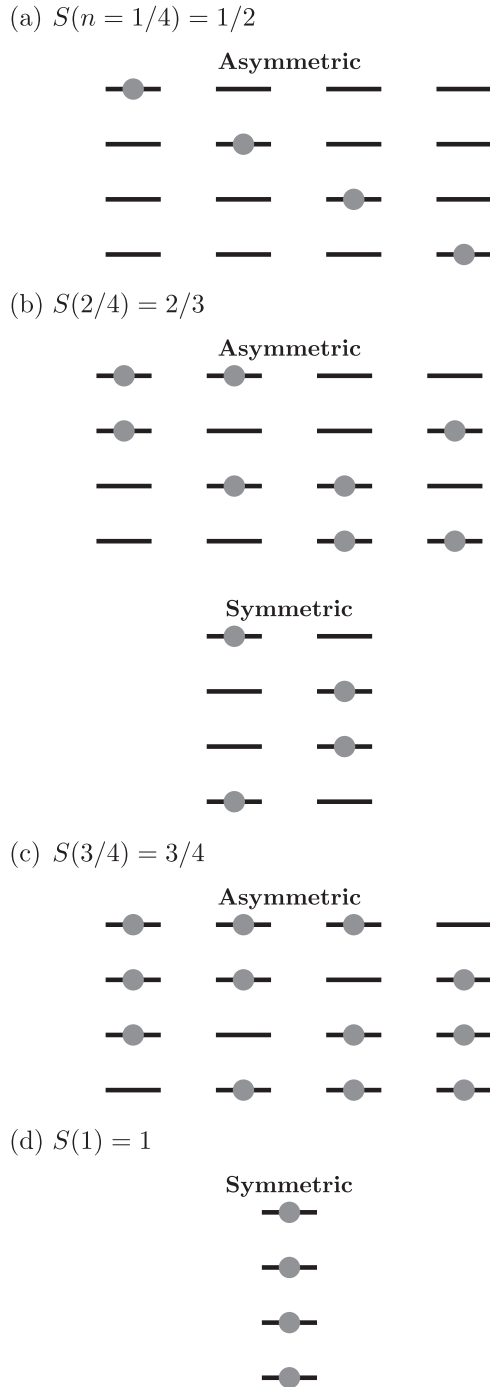


FIG. 3. Overview of all possible on-site impurity configurations for a single unit cell with four layers. The maximum number of impurities (indicated by the gray circles) is $N_{\max} = 4$. For each number of impurities N we included the corresponding symmetric share $S(n = N/N_{\max})$.

scattering potential is completely antisymmetric, we simply obtain $A_{\text{po}}(n) = 1$. Furthermore, as indicated in Fig. 4, the shares for on-site and intercalated impurities evolve in the same way as a function of the filling n .

We now examine which orbital wave functions are affected by the different impurity scattering matrices. To this extent we transform the symmetric and antisymmetric matrices

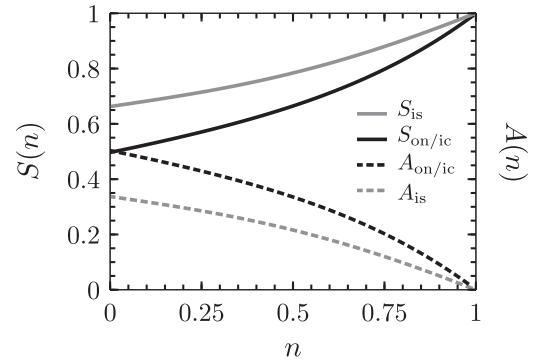


FIG. 4. Evolution of the symmetric share of impurity configurations, $S(n)$ (solid lines), as a function of the filling $n = N/N_{\max}$ for $N_{uc} \gg 1$. The difference between on-site (on), interstitial (is), and intercalated (ic) configurations is illustrated in Fig. 2. The dashed lines represent the antisymmetric shares given by $A(n) = 1 - S(n)$.

ces [Eqs. (14) and (15)] to the $\{P1_z^+, P1_z^-, P2_z^+, P2_z^-\}$ basis by evaluating $\hat{U}^\dagger \hat{V} \hat{U}$, with \hat{U} given by Eq. (4). We obtain for the symmetric scattering matrices

$$\hat{V}'_{S,1} = \begin{pmatrix} 0 & 0 & 0 & 0 \\ 0 & 0 & 0 & 0 \\ 0 & 0 & V & 0 \\ 0 & 0 & 0 & V \end{pmatrix}, \quad \hat{V}'_{S,2} = \begin{pmatrix} V & 0 & 0 & 0 \\ 0 & V & 0 & 0 \\ 0 & 0 & 0 & 0 \\ 0 & 0 & 0 & 0 \end{pmatrix}, \quad (20)$$

while the purely antisymmetric matrices are

$$\hat{V}'_{A,1} = \begin{pmatrix} 0 & 0 & 0 & 0 \\ 0 & 0 & 0 & 0 \\ 0 & 0 & 0 & V \\ 0 & 0 & V & 0 \end{pmatrix}, \quad \hat{V}'_{A,2} = \begin{pmatrix} 0 & V & 0 & 0 \\ V & 0 & 0 & 0 \\ 0 & 0 & 0 & 0 \\ 0 & 0 & 0 & 0 \end{pmatrix}. \quad (21)$$

As discussed in the previous section, the ultimate low-energy description of the electronic states can be cast in terms of two orbitals. From Eqs. (20) and (21), we see that the effective scattering matrices are going to depend on the choice of orbitals. In particular, some of the scattering matrices vanish in the low-energy basis. A summary of the reduced scattering matrices for all possible choices of two low-energy states is given in Table IV. Note that for orbitals involving different types of atoms, $\{P1_z^\alpha, P2_z^{\alpha'}\}$, all antisymmetric scattering matrices are zero in the low-energy basis. On the contrary, if the combinations involve the same type of atom, meaning $\{P1_z^+, P1_z^-\}$ and $\{P2_z^+, P2_z^-\}$, both the symmetric and

TABLE IV. Explicit form of the symmetric and antisymmetric scattering matrices for a particular two-orbital basis chosen from $\{P1_z^+, P1_z^-, P2_z^+, P2_z^-\}$, with $\alpha, \alpha' \in \{+, -\}$. Pauli matrices acting in orbital space are denoted by $\hat{\tau}_i$ with $i \in \{1, 2, 3\}$, where $\hat{\tau}_0$ corresponds to the identity matrix.

Two-orbital basis	$\hat{V}'_{S,1}$	$\hat{V}'_{S,2}$	$\hat{V}'_{A,1}$	$\hat{V}'_{A,2}$
$\{P1_z^+, P1_z^-\}$	0	$\hat{\tau}_0$	0	$\hat{\tau}_1$
$\{P2_z^+, P2_z^-\}$	$\hat{\tau}_0$	0	$\hat{\tau}_1$	0
$\{P1_z^\alpha, P2_z^{\alpha'}\}$	$\hat{\tau}_0 - \hat{\tau}_3$	$\hat{\tau}_0 + \hat{\tau}_3$	0	0

antisymmetric matrices are finite, as illustrated in Fig. 1. In the next section, we will analyze the implications of these findings regarding the renormalization of the superconducting temperature.

IV. RENORMALIZATION OF T_c

Within the standard self-consistent Born approximation, the reduction of the critical temperature in the presence of impurities for simple superconductors can be cast as [49]

$$\log_{10} \left(\frac{T_c}{T_{c0}} \right) = \Psi \left(\frac{1}{2} \right) - \Psi \left(\frac{1}{2} + \frac{1}{4\pi\tau_{\text{eff}}T_c} \right), \quad (22)$$

with $\Psi(x)$ denoting the digamma function and τ_{eff} the effective scattering rate defined as

$$\tau_{\text{eff}}^{-1} = \tau_n^{-1} - \tau_{\text{sc}}^{-1}, \quad (23)$$

in terms of the normal (τ_n) and superconducting (τ_{sc}) scattering rates. Below we begin by discussing how τ_n and τ_{sc} are obtained for complex superconductors with two orbital degrees of freedom contributing to a single Fermi surface. In Sec. IV C, we then discuss different scenarios with specific choices of orbitals and impurity location.

A. The normal scattering rate

The influence of impurity scattering on the electronic system is described by the renormalization of the Green's function, which we calculate by solving Dyson's equation [50],

$$\hat{G}^{-1}(\mathbf{k}, i\omega_n) = \hat{G}_0^{-1}(\mathbf{k}, i\omega_n) - \hat{\Sigma}_1(\mathbf{k}, i\omega_n). \quad (24)$$

Here we introduced the bare Green's function $\hat{G}_0(\mathbf{k}, i\omega_n)$ and self-energy $\hat{\Sigma}_1(\mathbf{k}, i\omega_n)$ of the normal state, which depend in general on the wave vector \mathbf{k} and the fermionic Matsubara frequencies $\omega_n = (2n + 1)\pi k_B T$. The bare Green's function is defined as

$$\hat{G}_0^{-1}(\mathbf{k}, i\omega_n) = i\omega_n \hat{\tau}_0 \otimes \hat{\sigma}_0 - \hat{H}(\mathbf{k}), \quad (25)$$

with $\hat{H}(\mathbf{k})$ given by Eq. (5). Using the Born approximation and assuming isotropic scattering, the self-energy has no \mathbf{k} dependence and takes the form

$$\hat{\Sigma}_1(i\omega_n) = \sum_i n_i \hat{V}_i \int \frac{d^3k}{(2\pi)^3} \hat{G}(\mathbf{k}, i\omega_n) \hat{V}_i, \quad (26)$$

where \hat{V}_i are the different scattering matrices in the two-orbital basis, as summarized in Table IV. After inverting Eq. (25), inserting the result in the equation for the self-energy, and solving the Dyson's equation self-consistently, we end up with a renormalization of the Matsubara frequencies (more details of this calculation are presented in the Appendix, which allows us to identify the normal-state scattering rate [24],

$$\tau_n^{-1} = \sum_i \frac{\pi}{2} V_i^2 N(0) n_i X_i(n) \left[1 + \sum_{a,b} C_{n,i}^{ab} \langle \hat{h}_{ab}(\mathbf{k}) \rangle^2 \right], \quad (27)$$

with $N(0)$ denoting the density of states at the Fermi level, V_i the magnitude of the scattering potential, and $X_i(n) = \{S_i(n), A_i(n)\}$ depending on the specific impurity potential \hat{V}_i , as indicated in Table IV. The factors $C_{n,i}^{ab}$ are equal to +1

TABLE V. Explicit values of the factors $C_{n,i}^{ab} = \pm 1$ and $C_{\text{sc},i}^{ab} = \pm 1$, which encode the commutation relations between the scattering potentials \hat{V}_i' and $h_{ab}(\mathbf{k})$ or d_{ab} , respectively. These factors appear in the equations of the normal-state [Eq. (27)] and superconducting [Eq. (31)] scattering rates. We assume an effective two-orbital model with OP or EP basis states. The scattering matrices in the low-energy model for each of these cases are contained in Table IV. Note that in the upper panel we have only included the (a, b) terms, which can belong to the A_{1g} representation, since they do not vanish after a FS average and ultimately contribute to the normal-state scattering rate.

		$C_{n,i}^{ab}$		
		\hat{V}_i'		
(a, b)		$\hat{\tau}_0$	$\hat{\tau}_1$	$\hat{\tau}_3$
(3,0)		+1	-1	+1
(1,0)		+1	+1	-1
		$C_{\text{sc},i}^{ab}$		
		\hat{V}_i'		
$[a, b]$		$\hat{\tau}_0$	$\hat{\tau}_1$	$\hat{\tau}_3$
[0,0]		+1	+1	+1
[3,0]		+1	-1	+1
[2,3]		+1	-1	-1
[1,0]		+1	+1	-1
[2,1]		+1	-1	-1
[2,2]		+1	-1	-1

(-1), if the corresponding term (a, b) in the normal-state Hamiltonian [Eq. (5)] commutes (anticommutes) with the scattering potential \hat{V}_i . Here $\langle f(\mathbf{k}) \rangle$ denotes the average over the Fermi surface of the function $f(\mathbf{k})$. Note that the sum of all symmetry-allowed pairs (a, b) excludes (0,0) and that the coefficients are normalized,

$$\sum_{a,b} \hat{h}_{ab}^2(\mathbf{k}) = 1. \quad (28)$$

Moreover, we implicitly assume a weak momentum-dependence of the scattering rate such that we can simply consider its FS average. In Table V we list the values of $C_{n,i}^{ab}$ for the all scattering potentials $\hat{V}_i = \hat{\tau}_0, \hat{\tau}_1, \hat{\tau}_3$. Note that we have to distinguish between OP and EP basis states, since the structure of the normal-state Hamiltonian is different for the EP or OP scenarios, as can be seen from Tables I and II. In particular, the (1,0) term is allowed in the normal-state Hamiltonian of a model with EP orbitals, but not with OP orbitals.

B. The superconducting scattering rate

In the superconducting state, we additionally have to take into account the renormalization of the anomalous Green's function $\hat{F}(\mathbf{k}, i\omega_n)$, which incorporates the pairing potential. Since we are only interested in the change of T_c , we can restrict ourselves to linear order in the gap function. The anomalous Green's function is then simply given by

$$\begin{aligned} \hat{F}(\mathbf{k}, i\omega_n) \approx & -\hat{G}(\mathbf{k}, i\omega_n) [\hat{\Delta}(\mathbf{k}) + \hat{\Sigma}_2(i\omega_n)] \\ & \times \hat{G}^T(-\mathbf{k}, -i\omega_n), \end{aligned} \quad (29)$$

where $\hat{\Delta}(\mathbf{k})$ is given by Eq. (6). We introduced the self-energy of the superconducting state $\hat{\Sigma}_2(i\omega_n)$, which in the Born approximation is defined as

$$\hat{\Sigma}_2(i\omega_n) = - \sum_i n_i \hat{V}_i \int \frac{d^3k}{(2\pi)^3} \hat{F}(\mathbf{k}, i\omega_n) \hat{V}_i^\dagger. \quad (30)$$

Analogously to before, we calculate first the anomalous Green's function and the corresponding self-energy. Solving then everything self-consistently enables us to find the renormalization of the pairing potential. From here on, we restrict ourselves to purely unconventional states, i.e., the non- A_{1g} s -wave gap functions. This allows us to directly obtain closed-form solutions for the scattering rates. Of course, the framework can also be extended to the A_{1g} channel. However, one then has to account for a superposition of multiple superconducting components, which we want to avoid here. Note that the equation above also makes clear that any order parameter with a nontrivial, symmetry-enforced \mathbf{k} dependence would lead to no renormalization of the order parameter, as the superconducting self-energy is zero after the sum over momenta is performed.

Neglecting interband pairing contributions we finally obtain for the superconducting scattering rate [24]

$$\tau_{sc}^{-1} = \sum_i \frac{\pi}{2} V_i^2 N(0) n_i X_i(n) C_{sc,i}^{ab} [1 - \langle F_C \rangle], \quad (31)$$

where $C_{sc,i}^{ab}$ is equal to +1 (−1), if the scattering potential \hat{V}_i commutes (anticommutes) with the particular gap function labeled as $[a, b]$ [Eq. (6)]. The values for all different s -wave superconducting states and scattering potentials are summarized in Table V. Note that the EP scenario has less active scattering matrices if compared to the OP scenario. In Eq. (31) we introduced the normalized average of the fitness function,

$$\langle F_C \rangle = \left\langle \frac{||\hat{F}_C(\mathbf{k})||^2}{\sum_{(a,b) \neq (0,0)} h_{ab}^2(\mathbf{k})} \right\rangle, \quad (32)$$

with the fitness matrix [39,41] given by

$$\hat{F}_C(\mathbf{k}) = \hat{H}(\mathbf{k}) \hat{\Delta}(\mathbf{k}) - \hat{\Delta}(\mathbf{k}) \hat{H}^T(-\mathbf{k}). \quad (33)$$

In Table VI we provide an overview of the terms (a, b) in the normal-state Hamiltonian, which contribute to a finite fitness function for the different pairing channels of interest labeled as $[a, b]$. As before, we also include the possibility of OP and EP basis states.

C. Analysis of three scenarios

In the following, we will use these results to analyze qualitatively the impurity-induced renormalization of the superconducting critical temperature for three generic scenarios of multilayered superconductors. The first example, which is about OP basis states originating from distinct types of atoms, is most closely related to the Bi_2Se_3 -related superconductors. In the second and third examples, we then discuss how the renormalization changes if the states have EP or have OP but originate from the same type of atoms. For all of these instances we consider on-site, interstitial, intercalated, and polar impurity configurations.

TABLE VI. The terms (a, b) of the normal-state Hamiltonian [Eq. (5)], contributing to the finite fitness function as $F_C(\mathbf{k}) = \sum_{a,b} \hat{h}_{ab}^2(\mathbf{k})$, for the corresponding s -wave superconducting states labeled as $[a, b]$ [Eq. (6)] in both OP and EP scenarios.

$\hat{F}_C^{\text{OP}}(\mathbf{k})$		
$[a, b]$	Irrep	(a, b)
[0,0]	A_{1g}	
[3,0]	A_{1g}	(2,0),(1,1),(1,2),(1,3)
[2,3]	A_{1u}	(3,0),(1,3)
[1,0]	A_{2u}	(3,0),(2,0)
[2,1]	E_u	(3,0),(1,2)
[2,2]	E_u	(3,0),(1,1)
$\hat{F}_C^{\text{EP}}(\mathbf{k})$		
[0,0]	A_{1g}	
[3,0]	A_{1g}	(1,0),(2,1),(2,2),(2,3)
[1,0]	A_{1g}	(3,0),(2,1),(2,2),(2,3)
[2,3]	A_{2g}	(1,0),(3,0),(2,1),(2,2)
[2,1]	E_g	(1,0),(3,0),(2,2),(2,3)
[2,2]	E_g	(1,0),(3,0),(2,1),(2,3)

1. OP orbitals from different atoms

For concreteness, here we assume the low-energy orbitals are $\{P1_z^+, P2_z^-\}$, the first associated with an even parity orbital originating from Bi atoms, the second associated with an odd parity orbital stemming from the Se atoms. From Table IV, we conclude that only the symmetric impurity configurations contribute to scattering. Thus, our first conclusion is that in the presence of purely polar impurities, which are entirely antisymmetric, the superconducting state is left untouched.

If the scattering is due to on-site or interstitial defects, the situation changes and we have two finite scattering processes in the effective low-energy model:

$$\hat{V}'_{S,1} = \hat{\tau}_0 - \hat{\tau}_3, \quad (34)$$

$$\hat{V}'_{S,2} = \hat{\tau}_0 + \hat{\tau}_3. \quad (35)$$

The overall impurity potential, which effectively renormalizes the order parameter, corresponds to a superposition of these. For random impurity distributions, the two scattering matrices are equally likely, and their average is ultimately given by the identity matrix $\hat{\tau}_0$. This leads to scattering rates given by

$$\tau_{n,i}^{-1} = \frac{\pi}{2} V_i^2 N(0) n S_i(n) (1 + \langle \hat{h}_{30} \rangle^2) \quad (36)$$

and

$$\tau_{sc,i}^{-1} = \frac{\pi}{2} V_i^2 N(0) n S_i(n) (1 - \langle F_C^{\text{OP}} \rangle), \quad (37)$$

where $i = \{\text{on, is}\}$. Here the \mathbf{k} dependence is implicit inside the brackets denoting the averages over the Fermi surface. Combining both equations leads to an effective scattering rate equal to

$$\tau_{\text{eff},i}^{-1} = \frac{\pi}{2} V_i^2 N(0) n S_i(n) (\langle \hat{h}_{30} \rangle^2 + \langle F_C^{\text{OP}} \rangle). \quad (38)$$

The first term inside the brackets is the same for all pairing symmetries. Thus, the difference between the effective scattering rate for different superconducting states is entirely

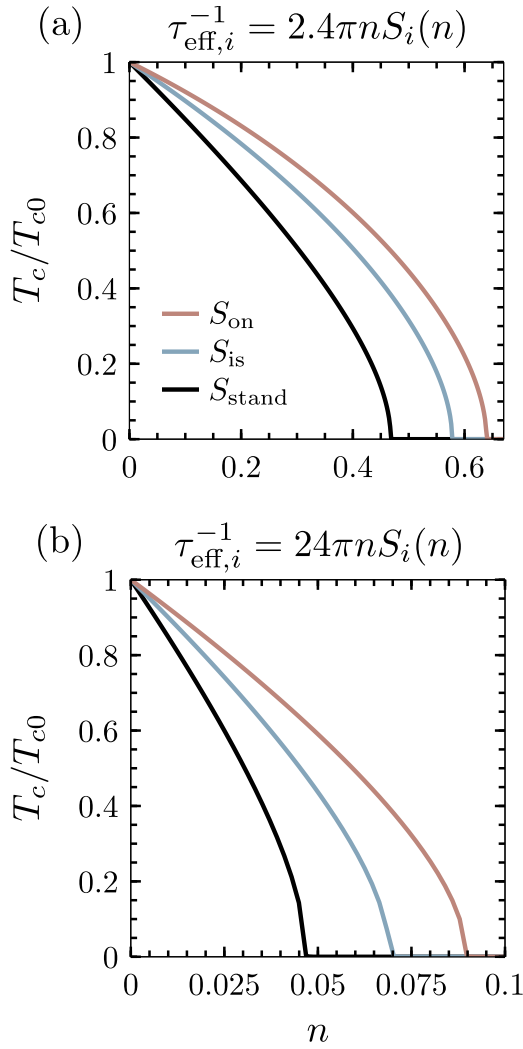


FIG. 5. Suppression of the normalized superconducting transition temperature T_c/T_{c0} versus the impurity concentration n , if only the symmetric share $S_i(n)$ of impurity distributions contributes to scattering, calculated from Eqs. (22) and (38). The standard case corresponds to the situation where the share of symmetric configurations stays constant as a function of the filling, i.e., $S_{\text{stand}} = 1$. For the top (bottom) figure we choose a small (large) prefactor to the scattering rate, corresponding to a weak (strong) scattering potential.

governed by the average of the respective fitness function. As we can infer from Table VI, all gap functions have a finite fitness measure, whose size depends on the details of the microscopic Hamiltonian. This aspect was already emphasized in previous works [24–26]. However, we also observe that the evolution of the share of symmetric configurations, $S_i(n)$, affects the scattering rate, which is a feature that does not depend on the structure of the Hamiltonian, but on the distribution of impurities. The influence of $S_i(n)$ on the renormalization of T_c is illustrated in Fig. 5. As expected from the shape of $S_i(n)$ (Fig. 4), we obtain that all superconducting states are more sensitive to interstitial than on-site defects (assuming same magnitude of the scattering potential on the sites). Furthermore, we note that in the case of strong on-site or interstitial impurity potentials, for which the superconduct-

ing state is suppressed by small impurity concentrations, there is an enhancement of the critical concentration by a maximum factor of approximately two [illustrated by Fig. 5(b)].

For intercalated configurations, the impurities can only occupy the first and fourth layer. Hence, the only finite scattering matrix in the low-energy model is given by $\hat{V}_{S,1}$ [Eq. (34)], which does not square to the identity matrix. This has important consequences for the scattering rates. First of all, since the gap functions not belonging to A_{1g} commute (anticommute) with $\hat{\tau}_0$ ($\hat{\tau}_3$), the superconducting scattering rate vanishes, i.e., $\tau_{\text{sc,ic}}^{-1} = 0$. In contrast, the normal-state scattering rate is finite because all terms of the averaged Green's function fully commute with the scattering potential. The effective scattering rate is therefore equal to

$$\tau_{\text{eff,ic}}^{-1} = \tau_{\text{n,ic}}^{-1} = \pi V_{\text{ic}}^2 N(0) n S_{\text{ic}}(n) (1 - \langle \hat{h}_{30} \rangle)^2. \quad (39)$$

We find that the normalized mass imbalance term in the Hamiltonian, \hat{h}_{30} , is again an important factor that controls the renormalization of the superconducting state in the presence of impurities. However, in contrast to the cases of interstitial or on-site impurities, we obtain that a larger contribution of \hat{h}_{30} to the normal-state Hamiltonian actually leads to a smaller effective scattering rate. Depending on the details of the normal-state Hamiltonian this could have profound consequences on the suppression of T_c .

In order to make better connections with experiments, we would like to emphasize here that the critical temperature is usually investigated as a function of the residual resistivity in the normal state [16,19]. The residual resistivity is proportional to the normal-state scattering rate, so it is sensible to study the evolution of the critical temperature not only with respect to the impurity concentration, but also with respect to the normal-state scattering rate. We can write

$$\log_{10} \left(\frac{T_c}{T_{c0}} \right) = \Psi \left(\frac{1}{2} \right) - \Psi \left(\frac{1}{2} + \frac{1}{4\pi \tau_n T_c \tau_{\text{eff}}} \right), \quad (40)$$

such that the ratio τ_n/τ_{eff} can be thought of as the *effectiveness* of the impurities in the superconducting state. If this ratio is large (small) the superconducting critical temperature is suppressed faster (slower) than naively expected for a single-band superconductor. In the case of on-site and interstitial scenarios, we find for superconducting states in nontrivial irreps

$$\frac{\tau_n}{\tau_{\text{eff}}} = \frac{\langle F_C^{OP} \rangle + \langle \hat{h}_{30} \rangle^2}{1 + \langle \hat{h}_{30} \rangle^2}. \quad (41)$$

From this ratio, let us discuss two extreme limits. The first corresponds to $\langle \hat{h}_{30} \rangle \rightarrow 0$ such that $\tau_n/\tau_{\text{eff}} \rightarrow \langle F_C^{OP} \rangle$. In this limit, assuming OP orbitals we obtain $\langle F_C^{OP} \rangle = \langle \hat{h}_{ab}^2 \rangle$ for a single (a, b) term in the normal-state Hamiltonian (according to Table VI). If this term is dominant, $\tau_n/\tau_{\text{eff}} \rightarrow 1$ and the superconductor behaves as expected for simple single-band scenarios. On the other hand, if the specific (a, b) term is negligible, $\tau_n/\tau_{\text{eff}} \rightarrow 0$ and the superconducting state is suppressed at a much slower rate than expected from a naive estimation. The second limit corresponds to $\langle \hat{h}_{30} \rangle \rightarrow 1$, with all other $\langle \hat{h}_{ab}^2 \rangle \rightarrow 0$. In this case, the ratio $\tau_n/\tau_{\text{eff}} \rightarrow 1/2$ and the superconducting state is suppressed at impurity concentrations that are twice as large as the naively expected values.

For intercalated impurities the ratio $\tau_n/\tau_{\text{eff}} = 1$, meaning that the suppression of the superconducting state would follow the naive expectation for simple superconductors.

From this discussion, we can conclude that an arbitrarily robust unconventional superconducting state is possible in layered materials in the presence of on-site or interstitial impurities, for the scenario with OP orbitals stemming from distinct types of atoms under the condition that the (a, b) terms enumerated in Table VI (top) for each superconducting state are the least dominant terms in the normal-state Hamiltonian.

It is important at this point to highlight the role of the (3,0) mass-imbalance term, which contributes to a finite superconducting fitness for all unconventional order parameters not belonging to the A_{1g} representation. First, note that the order parameters considered here are all of interorbital nature. If we start with the most plain type of electronic structure with only the (0,0) term, we find four spin and orbital degenerate bands. This configuration is associated with the most advantageous scenario for interorbital pairing, as we fall in the case of intraband pairing. Once we turn on the (3,0) term, the orbital degeneracy is lost and now interorbital pairing is only possible through interband pairing, a suboptimal scenario. Note also that the other terms contributing to the superconducting fitness, displayed in Table VI (top), are symmetric (antisymmetric) in the orbital degree of freedom for every odd-parity order parameter, if the superconducting order parameter is antisymmetric (symmetric) in the orbital degree of freedom. This highlights the incompatibility of these terms with the respective superconducting state.

This scenario with OP orbitals from different atoms is the one associated with the physics of materials belonging to the family of Bi_2Se_3 . They have attracted a lot of attention given their topological properties. As discussed in Ref. [28], the condition for band inversion is given by $M_0M_1 < 0$ [parameters in Table I associated with the (3,0) term]. This constraint makes the (3,0) term arbitrarily small for selected k_z values. A small (3,0) term is a necessary condition for the development of an unconventional superconducting state that is arbitrarily robust [in case the extra (a, b) term contributing to \hat{F}_C is also negligible]. Here we can conclude that electronic structure parameters related to nontrivial topology guarantee a more robust superconducting state.

Let us analyze next how these qualitative results change for EP basis states.

2. EP orbitals from different atoms

According to Table IV, for basis states with EP, such as $\{P2_z^+, P2_z^-\}$, we obtain the same scattering matrices as in the previous subsection. This means that polar impurities play again no role in the renormalization of the superconducting state. The only differences compared to the OP case arise due to the changes in the structure of the Hamiltonian. Naturally, these differences are more of quantitative than of qualitative nature.

For example, for on-site or interstitial distributions we find

$$\tau_{n,i}^{\prime-1} = \frac{\pi}{2} V_i^2 N(0) n S_i(n) (1 + \langle \hat{h}_{30} \rangle^2 + \langle \hat{h}_{10} \rangle^2) \quad (42)$$

and

$$\tau_{sc,i}^{\prime-1} = \frac{\pi}{2} V_i^2 N(0) n S_i(n) (1 - \langle F_C^{\text{EP}} \rangle), \quad (43)$$

with $i = \{\text{on}, \text{is}\}$. Consequently, the effective scattering rate becomes

$$\tau_{\text{eff},i}^{\prime-1} = \frac{\pi}{2} V_i^2 N(0) n S_i(n) (\langle \hat{h}_{30} \rangle^2 + \langle \hat{h}_{10} \rangle^2 + \langle F_C^{\text{EP}} \rangle). \quad (44)$$

The only difference to Eq. (38) is therefore a different prefactor determined by the microscopic structure of the Hamiltonian. Surprisingly, for intercalated impurities we obtain exactly the same results as before, since the \hat{h}_{10} term of the Hamiltonian anticommutes with $\hat{\tau}_3$. Consequently, its contribution vanishes in the normal-state scattering rate and we again end up with Eq. (39). From this we can deduce that disorder located in the vdW gap has the same effect in OP and EP two-orbital models stemming from distinct types of atoms.

For the EP orbitals scenario, the discussion of the evolution of the critical temperature as a function of the normal-state scattering rate is similar to the one given above for the OP scenario. We can again conclude that an arbitrarily robust unconventional superconducting state is theoretically possible in layered materials with EP orbitals stemming from distinct types of atoms under the condition that the (a, b) terms enumerated in Table VI (bottom) are not the dominant terms in the normal-state Hamiltonian. Note that the number of terms in Table VI is four, in contrast to two for the OP scenario. This means that superconductors stemming from Fermi surfaces formed by EP orbitals are generally much less likely to be robust than the ones stemming from OP orbitals. The condition for robustness would require four out of the six symmetry-allowed terms in the normal-state Hamiltonian to be negligible.

3. OP orbitals from the same atoms

If the states occupy the same type of atoms, as is the case for $\{P2_z^+, P2_z^-\}$, the renormalization changes substantially. From Table IV, we see that polar impurities, with scattering potential in the low-energy basis given by $\hat{\tau}_1$, now suppress the superconducting state. The corresponding scattering rates read

$$\tau_{n,\text{po}}^{\prime-1} = \frac{\pi}{2} V_{\text{po}}^2 N(0) n A_{\text{po}}(n) (1 - \langle \hat{h}_{30} \rangle^2) \quad (45)$$

and

$$\tau_{sc,\text{po}}^{\prime-1} = C_{sc,\text{po}}^{ab} \frac{\pi}{2} V_{\text{po}}^2 N(0) n A_{\text{po}}(n) (1 - \langle F_C^{\text{OP}} \rangle), \quad (46)$$

where we obtain a different overall sign in the last equation due to the $C_{sc,\text{po}}^{ab}$ factors (Table V). Subtracting the scattering rates leads now to

$$\tau_{\text{eff},\text{po}}^{\prime-1} = \frac{\pi}{2} V_{\text{po}}^2 N(0) n A_{\text{po}}(n) \times \left[1 - \langle \hat{h}_{30} \rangle^2 - C_{sc,\text{po}}^{ab} (1 - \langle F_C^{\text{OP}} \rangle) \right]. \quad (47)$$

Note that again the scattering rates for different gap functions merely differ by the overall factor in the square brackets. Assuming the system is purely populated by polar impurities such that the share of antisymmetric configurations stays constant, i.e., $A_{\text{po}}(n) = 1$, Eq. (47) yields a renormalization which

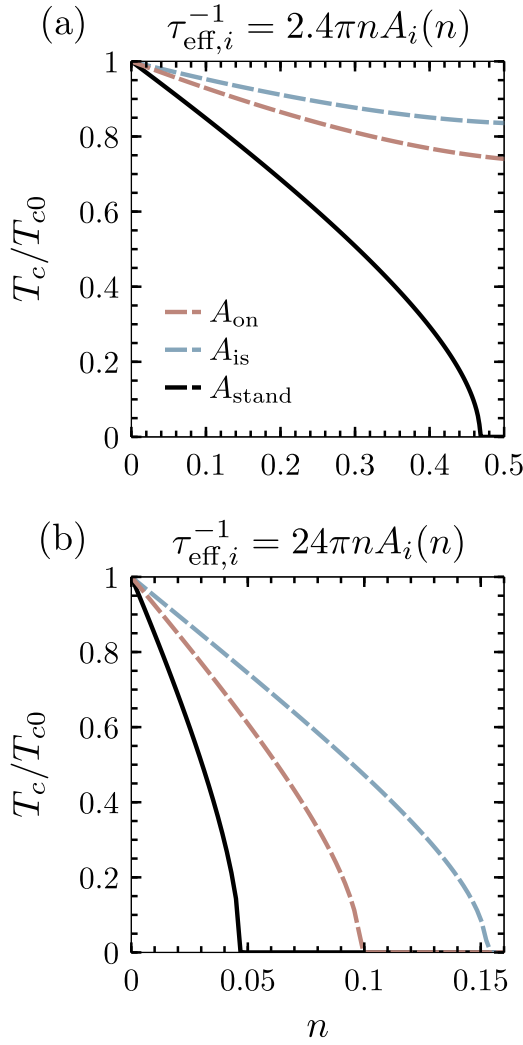


FIG. 6. Suppression of the normalized critical temperature T_c/T_{c0} as a function of the impurity filling fraction n , if only the antisymmetric share $A(n)$ of impurity distributions contributes, calculated from Eqs. (22) and (51). We used the antisymmetric shares $A_{\text{on/is}}$ calculated in Sec. III and $A_{\text{stand}} = 1$. We again choose a small and large prefactor to illustrate the effects of a weak and strong scattering potential, respectively.

only depends on the details of the microscopic Hamiltonian. In Fig. 6, we show how this feature can influence the robustness of the superconducting state irrespective of the expansion coefficients of the normal-state Hamiltonian.

For on-site, interstitial, and intercalated impurities the scattering rates contain both symmetric and antisymmetric shares.

We obtain

$$\tau_{n,i}''^{-1} = \frac{\pi}{2} V_i^2 N(0) n [S_i(n)(1 + \langle \hat{h}_{30} \rangle^2) + A_i(n)(1 - \langle \hat{h}_{30} \rangle^2)] \quad (48)$$

and

$$\tau_{\text{sc},i}''^{-1} = \frac{\pi}{2} V_i^2 N(0) n [S_i(n)(1 - \langle F_C^{\text{OP}} \rangle) + C_{\text{sc},i}^{ab} A_i(n)(1 - \langle F_C^{\text{OP}} \rangle)], \quad (49)$$

with $i = \{\text{on, is, ic}\}$. Note that not all non- A_{1g} gap functions commute with $\hat{\tau}_1$; hence we have to include the different $C_{\text{sc},i}^{ab}$ in the second line of the last equation. The effective scattering rate is

$$\tau_{\text{eff},i}''^{-1} = \frac{\pi}{2} V_i^2 N(0) n \{ 1 + [S_i(n) - A_i(n)] \langle \hat{h}_{30} \rangle^2 - (1 - \langle F_C^{\text{OP}} \rangle) [S_i(n) + C_{\text{sc},i}^{ab} A_i(n)] \}, \quad (50)$$

where we used $S_i(n) + A_i(n) = 1$. We observe that if the states originate from the same layers, we cannot in general separate the symmetric and antisymmetric shares from the microscopic details of the Hamiltonian. Similar to the previous cases, we find that the explicit structure of the shares influences the scattering rate. Analyzing to what extent, however, requires a more detailed calculation of the microscopic parameters, which is not the scope of this paper. Nevertheless, we can deduce from Eq. (50) that there might be a fine-tuned value of parameters, for which only the antisymmetric share contributes. Rewriting Eq. (50),

$$\tau_{\text{eff},i}''^{-1} = \frac{\pi}{2} V_i^2 N(0) n \{ S_i(n) (\langle \hat{h}_{30} \rangle^2 + \langle F_C^{\text{OP}} \rangle) + A_i(n) [1 - \langle \hat{h}_{30} \rangle^2 - (1 - \langle F_C^{\text{OP}} \rangle) C_{\text{sc},i}^{ab}] \}, \quad (51)$$

we see that this is the case if

$$\langle \hat{h}_{30} \rangle^2 + \langle F_C^{\text{OP}} \rangle = 0. \quad (52)$$

Assuming $\langle F_C^{\text{OP}} \rangle \rightarrow 0$ and $C_{\text{sc},i}^{ab} = -1$, the renormalization of the critical temperature is governed by the antisymmetric share of scattering potentials, as shown in Fig. 6. Intriguingly, we observe that the robustness of the superconducting state increases drastically for small scattering potential, since the share of antisymmetric configurations is reduced as the system is gradually filled with on-site or interstitial impurities. As an aside, we also have to emphasize that for intercalated impurities only our basis choice of $\{P2_z^+, P2_z^-\}$ leads to the expression given in Eq. (50). Naturally, choosing a basis which originates from the inner layers yields no renormalization for intercalated distributions.

Continuing with the discussion of the evolution of the critical temperature as a function of the normal-state scattering rate, we find now according to Eq. (40)

$$\frac{\tau_n}{\tau_{\text{eff}}} = \frac{1 + [S_i(n) - A_i(n)] \langle \hat{h}_{30} \rangle^2 - (1 - \langle F_C^{\text{OP}} \rangle) [S_i(n) + C_{\text{sc},i}^{ab} A_i(n)]}{1 + [S_i(n) - A_i(n)] \langle \hat{h}_{30} \rangle^2}. \quad (53)$$

As before, we want to consider two extreme limits. The first concerns $\langle \hat{h}_{30} \rangle \rightarrow 0$, in which case the ratio simplifies to

$$\frac{\tau_n}{\tau_{\text{eff}}} = 1 - (1 - \langle F_C^{\text{OP}} \rangle) [S_i(n) + C_{\text{sc},i}^{ab} A_i(n)], \quad (54)$$

and becomes equal to $\langle F_C^{\text{OP}} \rangle$ for $C_{\text{sc},i}^{ab} = +1$. As the normalized fitness parameter satisfies $0 < \langle F_C^{\text{OP}} \rangle < 1$, the ratio is necessarily smaller than one, and the superconducting state is generally less suppressed than in the naive single-band scenario. For $C_{\text{sc},i}^{ab} = -1$, the form of the ratio is not as simple, but the conclusion, based on the fact that $0 \leq \tau_n/\tau_{\text{eff}} \leq 1$, is the same. Overall, we find that for the scenario of two OP orbitals stemming from the same type of atoms, the conclusion that the superconducting state can be arbitrarily robust, as long as the normal-state Hamiltonian terms (a, b) contributing to $\langle F_C^{\text{OP}} \rangle$ are negligible, is essentially the same as for the case of two OP orbitals stemming from distinct types of atoms.

V. CONCLUSION

Inspired by the open questions concerning the robustness of the superconducting state found in materials belonging to the family of doped Bi_2Se_3 , we have investigated the effects of the impurity location and orbital content at the Fermi surface on the critical temperature of layered superconductors. We started revisiting the microscopic description in the layer basis to faithfully account for four distinct impurity configurations: on-site, interstitial, intercalated, and polar. After moving to the orbital basis by projecting our model into two low-lying degrees of freedom, we found three fundamentally distinct effective two-orbital bases. This allowed us to discuss whether the symmetric and antisymmetric shares of the scattering potentials were active or inactive in each of these cases. In particular, we find that choosing two orbitals stemming from distinct types of atoms, the antisymmetric part of the scattering potential is inactive, irrespective of the relative parity of the orbitals. We then elaborated on the renormalization of the superconducting critical temperature within the self-consistent Born approximation by providing closed-form expressions for the effective scattering rate. For simplicity, we restricted ourselves here to the unconventional states not belonging to the A_{1g} representation. We obtain that the effective scattering rate depends on three important properties: (i) the commutation/anticommutation relation between the normal-state Hamiltonian and the scattering potential; (ii) the commutation/anticommutation relation between the superconducting order parameter and the scattering potential; and (iii) the commutation/anticommutation relation between the normal-state Hamiltonian and the superconducting order parameter (known as the superconducting fitness measure).

For the main case of interest, OP orbitals stemming from distinct types of atoms, we observe that purely polar impurities do not suppress the superconducting state. Moreover, on-site and interstitial impurities behave qualitatively the same: the superconducting state is more robust for the smaller mass imbalance, (3,0) term, in the normal-state Hamiltonian. Nevertheless, on-site impurities are generally less effective in suppressing the superconducting state compared to interstitial impurities (assuming the magnitude of the scattering potential

and the normal-state Hamiltonian are the same). This is due to the distinct evolution of the symmetric share as a function of doping. The superconducting state is also possibly more robust than usual for intercalated impurities, but now the robustness is enhanced if the contribution of the (3,0) term to the normal-state Hamiltonian increases.

We also conclude that superconductors emerging from Fermi surfaces formed by two OP orbitals are generally more robust than superconductors stemming from Fermi surfaces with EP orbitals. This effect is purely controlled by the fitness measure $\langle F_C \rangle$. Furthermore, considering two OP orbitals stemming from the same type of atoms as the basis states, we conclude that these are affected by purely polar impurities, in contrast to the scenario where the orbitals stem from different types of atoms.

In addition, within the scenario of OP orbitals, we discovered a new mechanism to enhance the robustness of superconducting states. In case the antisymmetric share of the impurity potential is dominant, the superconducting state can also be exceptionally robust to on-site, interstitial, and intercalated impurities since the antisymmetric share decreases with doping.

Finally, we highlighted the difference in discussing the robustness of the superconducting state as a function of the impurity concentration or of the normal-state scattering rate. Our findings show that an enhanced robustness can be observed for both on-site and interstitial impurities when analyzing the critical temperature either as a function of impurity concentration or τ_n^{-1} . On the other hand, an enhanced robustness for intercalated impurities only appears when analyzing the evolution of the superconducting critical temperature with the impurity concentration. These results can have important implications for the interpretation of experiments and the identification of the impurity location in layered materials.

We believe our work provides an important starting point to answer the questions concerning the stability of superconducting states in the presence of impurities in layered materials. This work also opens further questions concerning the connections between the normal-state topology and the robustness of the superconducting state and the possibility of engineering the normal-state electronic structure to make superconductors less susceptible to disorder. We believe these are interesting directions for future work.

ACKNOWLEDGMENTS

We would like to thank Manfred Sgrist, Philip Brydon, and David C. Cavanagh for helpful discussions. A.R. acknowledges the financial support of the Swiss National Science Foundation through Ambizione Grant No. 186043 and B.Z. the financial support of the SNSF through Division II (Grant No. 184739).

APPENDIX: DERIVATION OF τ_n

Here we illustrate the derivation of the normal-state scattering rate τ_n introduced in Sec. IV A. Our starting point is Dyson's equation [50],

$$\hat{G}^{-1}(\mathbf{k}, i\omega_n) = \hat{G}_0^{-1}(\mathbf{k}, i\omega_n) - \hat{\Sigma}_1(\mathbf{k}, i\omega_n), \quad (\text{A1})$$

which contains the bare Green's function $\hat{G}_0(\mathbf{k}, i\omega_n)$ defined in Eq. (25) in the main text. Inserting the expression of $\hat{H}(\mathbf{k})$ given by Eq. (5), the renormalized Green's function in the band basis reads

$$\hat{G}(\mathbf{k}, i\omega_n) = \frac{1}{2} \sum_{j=\pm} \frac{1}{i\tilde{\omega}_{n,j} - E_{k,j}} \times \left(\hat{\tau}_0 \otimes \hat{\sigma}_0 + j \sum_{a,b} \hat{h}_{ab}(\mathbf{k}) \hat{\tau}_a \otimes \hat{\sigma}_b \right), \quad (\text{A2})$$

where $j = \pm 1$ denotes the band index, $\tilde{\omega}_n$ the renormalized Matsubara frequencies, and $E_{k,j}$ the band energies given by

$$E_{k,j} = h_{00}(\mathbf{k}) + j \sqrt{\sum_{a,b} h_{ab}^2(\mathbf{k})}. \quad (\text{A3})$$

Note that the sum over (a, b) in Eqs. (A2) and (A3) excludes $(0,0)$ and that we normalized the terms of the Hamiltonian:

$$\sum_{a,b} \hat{h}_{ab}^2(\mathbf{k}) = 1. \quad (\text{A4})$$

We should also emphasize that expressed in terms of the renormalized Matsubara frequencies the inverse of Eq. (A2) is equal to

$$\begin{aligned} \hat{G}^{-1}(\mathbf{k}, i\omega_n) &= \frac{i\tilde{\omega}_{n,+} + i\tilde{\omega}_{n,-} - 2h_{00}}{2} \hat{\tau}_0 \otimes \hat{\sigma}_0 \\ &+ \frac{i\tilde{\omega}_{n,+} - i\tilde{\omega}_{n,-} - 2\sqrt{\sum_{a,b} h_{ab}^2}}{2} \sum_{a,b} \hat{h}_{ab} \hat{\tau}_a \otimes \hat{\sigma}_b, \quad (\text{A5}) \end{aligned}$$

where we for once omitted writing down the explicit \mathbf{k} dependence of the $\hat{h}_{ab}(\mathbf{k})$ terms.

As discussed in the main text, we want to work in the Born approximation where the self-energy is given by

$$\hat{\Sigma}_1(i\omega_n) = \sum_i n_i \hat{V}_i \int \frac{d^3k}{(2\pi)^3} \hat{G}(\mathbf{k}, i\omega_n) \hat{V}_i, \quad (\text{A6})$$

with \hat{V}_i denoting the scattering matrices in the two-orbital basis. Inserting Eq. (A2) in Eq. (A6) and performing the integration over \mathbf{k} yields

$$\begin{aligned} \hat{\Sigma}_1(i\omega_n) &= -i \frac{\pi}{2} \text{sgn}(\tilde{\omega}_n) \sum_i n_i |V_i|^2 \sum_j N_j(0) \\ &\times \left(\hat{\tau}_0 \otimes \hat{\sigma}_0 + j \sum_{a,b} C_{n,i}^{ab} \langle \hat{h}_{ab}(\mathbf{k}) \rangle_j \hat{\tau}_a \otimes \hat{\sigma}_b \right), \quad (\text{A7}) \end{aligned}$$

where we introduced the density of states at the Fermi level for band j , $N_j(0)$. This equation is finally inserted in Dyson's equation [Eq. (A1)] along with the inverses of the bare and renormalized Green's functions. Since we have two equations, one multiplied by $\hat{\tau}_0 \otimes \hat{\sigma}_0$ and the other one by $\sum_{a,b} \hat{\tau}_a \otimes \hat{\sigma}_b$, we can add and subtract them to obtain

$$\begin{aligned} \tilde{\omega}_{n,+} &= \omega_n + \frac{\pi}{2} \text{sgn}(\tilde{\omega}_n) \sum_i n_i |V_i|^2 \sum_j N_j(0) \\ &\times \left(1 + j \sum_{a,b} C_{n,i}^{ab} \langle \hat{h}_{ab}(\mathbf{k}) \rangle_j^2 \right) \quad (\text{A8}) \end{aligned}$$

for the first band and

$$\begin{aligned} \tilde{\omega}_{n,-} &= \omega_n + \frac{\pi}{2} \text{sgn}(\tilde{\omega}_n) \sum_i n_i |V_i|^2 \sum_j N_j(0) \\ &\times \left(1 - j \sum_{a,b} C_{n,i}^{ab} \langle \hat{h}_{ab}(\mathbf{k}) \rangle_j^2 \right) \quad (\text{A9}) \end{aligned}$$

for the second band. Note that we have averaged the scattering rate over the Fermi surface, since we assume that its \mathbf{k} dependence is small. Most notably, we find that every even $h_{ab}(\mathbf{k})$ term of the Hamiltonian modifies the scattering. Restricting ourselves now to the upper band with index $j = +1$ we end up with the normal-state scattering rate shown in Eq. (27) of the main text.

-
- [1] P. Anderson, Theory of dirty superconductors, *J. Phys. Chem. Solids* **11**, 26 (1959).
- [2] P. W. Anderson, Structure of "triplet" superconducting energy gaps, *Phys. Rev. B* **30**, 4000 (1984).
- [3] A. A. Abrikosov and L. P. Gor'kov, On the theory of superconducting alloys. I. The electrodynamic of alloys at absolute zero, *Sov. Phys. JETP* **35**, 1090 (1959).
- [4] H. Suhl and B. T. Matthias, Impurity scattering in superconductors, *Phys. Rev.* **114**, 977 (1959).
- [5] Y. Dalichaouch, M. C. de Andrade, D. A. Gajewski, R. Chau, P. Visani, and M. B. Maple, Impurity Scattering and Triplet Superconductivity in UPt_3 , *Phys. Rev. Lett.* **75**, 3938 (1995).
- [6] A. P. Mackenzie, R. K. W. Haselwimmer, A. W. Tyler, G. G. Lonzarich, Y. Mori, S. Nishizaki, and Y. Maeno, Extremely Strong Dependence of Superconductivity on Disorder in Sr_2RuO_4 , *Phys. Rev. Lett.* **80**, 161 (1998).
- [7] K. Fujita, T. Noda, K. M. Kojima, H. Eisaki, and S. Uchida, Effect of Disorder Outside the CuO_2 Planes on T_c of Copper Oxide Superconductors, *Phys. Rev. Lett.* **95**, 097006 (2005).
- [8] Y. Senga and H. Kontani, Impurity effects in sign-reversing fully gapped superconductors: Analysis of FeAs superconductors, *J. Phys. Soc. Jpn.* **77**, 113710 (2008).
- [9] S. Onari and H. Kontani, Violation of Anderson's Theorem for the Sign-Reversing s -Wave State of Iron-Pnictide Superconductors, *Phys. Rev. Lett.* **103**, 177001 (2009).
- [10] Y. Wang, A. Kreisel, P. J. Hirschfeld, and V. Mishra, Using controlled disorder to distinguish s_{\pm} and s_{++} gap structure in Fe-based superconductors, *Phys. Rev. B* **87**, 094504 (2013).
- [11] S. Sasaki, K. Segawa, and Y. Ando, Superconductor derived from a topological insulator heterostructure, *Phys. Rev. B* **90**, 220504(R) (2014).

- [12] L. Andersen, Z. Wang, T. Lorenz, and Y. Ando, Nematic superconductivity in $\text{Cu}_{1.5}(\text{PbSe})_5(\text{Bi}_2\text{Se}_3)_6$, *Phys. Rev. B* **98**, 220512(R) (2018).
- [13] L. Andersen, A. Ramires, Z. Wang, T. Lorenz, and Y. Ando, Generalized Anderson's theorem for superconductors derived from topological insulators, *Sci. Adv.* **6**, eaay6502 (2020).
- [14] Y. S. Hor, A. J. Williams, J. G. Checkelsky, P. Roushan, J. Seo, Q. Xu, H. W. Zandbergen, A. Yazdani, N. P. Ong, and R. J. Cava, Superconductivity in $\text{Cu}_x\text{Bi}_2\text{Se}_3$ and Its Implications for Pairing in the Undoped Topological Insulator, *Phys. Rev. Lett.* **104**, 057001 (2010).
- [15] S. Yonezawa, K. Tajiri, S. Nakata, Y. Nagai, Z. Wang, K. Segawa, Y. Ando, and Y. Maeno, Thermodynamic evidence for nematic superconductivity in $\text{Cu}_x\text{Bi}_2\text{Se}_3$, *Nat. Phys.* **13**, 123 (2017).
- [16] M. Kriener, K. Segawa, S. Sasaki, and Y. Ando, Anomalous suppression of the superfluid density in the $\text{Cu}_x\text{Bi}_2\text{Se}_3$ superconductor upon progressive Cu intercalation, *Phys. Rev. B* **86**, 180505(R) (2012).
- [17] Y. Qiu, K. N. Sanders, J. Dai, J. E. Medvedeva, W. Wu, P. Ghaemi, T. Vojta, and Y. S. Hor, Time reversal symmetry breaking superconductivity in topological materials, [arXiv:1512.03519](https://arxiv.org/abs/1512.03519).
- [18] M. P. Smylie, H. Claus, U. Welp, W.-K. Kwok, Y. Qiu, Y. S. Hor, and A. Snezhko, Evidence of nodes in the order parameter of the superconducting doped topological insulator $\text{Nb}_x\text{Bi}_2\text{Se}_3$ via penetration depth measurements, *Phys. Rev. B* **94**, 180510(R) (2016).
- [19] M. P. Smylie, K. Willa, H. Claus, A. Snezhko, I. Martin, W.-K. Kwok, Y. Qiu, Y. S. Hor, E. Bokari, P. Niraula, A. Kayani, V. Mishra, and U. Welp, Robust odd-parity superconductivity in the doped topological insulator $\text{Nb}_x\text{Bi}_2\text{Se}_3$, *Phys. Rev. B* **96**, 115145 (2017).
- [20] M. Novak, S. Sasaki, M. Kriener, K. Segawa, and Y. Ando, Unusual nature of fully gapped superconductivity in In-doped SnTe , *Phys. Rev. B* **88**, 140502(R) (2013).
- [21] E. I. Timmons, S. Teknowijoyo, M. Kończykowski, O. Cavani, M. A. Tanatar, S. Ghimire, K. Cho, Y. Lee, L. Ke, N. H. Jo, S. L. Bud'ko, P. C. Canfield, P. P. Orth, M. S. Scheurer, and R. Prozorov, Electron irradiation effects on superconductivity in PdTe_2 : An application of a generalized Anderson theorem, *Phys. Rev. Research* **2**, 023140 (2020).
- [22] K. Michaeli and L. Fu, Spin-Orbit Locking as a Protection Mechanism of the Odd-Parity Superconducting State against Disorder, *Phys. Rev. Lett.* **109**, 187003 (2012).
- [23] Y. Nagai, Robust superconductivity with nodes in the superconducting topological insulator $\text{Cu}_x\text{Bi}_2\text{Se}_3$: Zeeman orbital field and nonmagnetic impurities, *Phys. Rev. B* **91**, 060502(R) (2015).
- [24] D. C. Cavanagh and P. M. R. Brydon, General theory of robustness against disorder in multiband superconductors, *Phys. Rev. B* **104**, 014503 (2021).
- [25] T. Sato and Y. Asano, Superconductivity in Cu-doped Bi_2Se_3 with potential disorder, *Phys. Rev. B* **102**, 024516 (2020).
- [26] D. Dentelski, V. Kozii, and J. Ruhman, Effect of interorbital scattering on superconductivity in doped Dirac semimetals, *Phys. Rev. Research* **2**, 033302 (2020).
- [27] D. C. Cavanagh and P. M. R. Brydon, Robustness of unconventional *s*-wave superconducting states against disorder, *Phys. Rev. B* **101**, 054509 (2020).
- [28] C.-X. Liu, X.-L. Qi, H. J. Zhang, X. Dai, Z. Fang, and S.-C. Zhang, Model Hamiltonian for topological insulators, *Phys. Rev. B* **82**, 045122 (2010).
- [29] Y.-R. Lin, M. Bagchi, S. Soubatch, T.-L. Lee, J. Brede, F. C. Bocquet, C. Kumpf, Y. Ando, and F. S. Tautz, Vertical position of Sr dopants in the $\text{Sr}_x\text{Bi}_2\text{Se}_3$ superconductor, *Phys. Rev. B* **104**, 054506 (2021).
- [30] Y.-L. Wang, Y. Xu, Y.-P. Jiang, J.-W. Liu, C.-Z. Chang, M. Chen, Z. Li, C.-L. Song, L.-L. Wang, K. He, X. Chen, W.-H. Duan, Q.-K. Xue, and X.-C. Ma, Structural defects and electronic properties of the Cu-doped topological insulator Bi_2Se_3 , *Phys. Rev. B* **84**, 075335 (2011).
- [31] Z. Li, M. Wang, D. Zhang, N. Feng, W. Jiang, C. Han, W. Chen, M. Ye, C. Gao, J. Jia, J. Li, S. Qiao, D. Qian, B. Xu, H. Tian, and B. Gao, Possible structural origin of superconductivity in Sr-doped Bi_2Se_3 , *Phys. Rev. Materials* **2**, 014201 (2018).
- [32] T. Shirasawa, M. Sugiki, T. Hirahara, M. Aitani, T. Shirai, S. Hasegawa, and T. Takahashi, Structure and transport properties of Cu-doped Bi_2Se_3 films, *Phys. Rev. B* **89**, 195311 (2014).
- [33] M. Wang, Y. Song, L. You, Z. Li, B. Gao, X. Xie, and M. Jiang, A combined method for synthesis of superconducting Cu doped Bi_2Se_3 , *Sci. Rep.* **6**, 22713 (2016).
- [34] T. Fröhlich, Z. Wang, M. Bagchi, A. Stunault, Y. Ando, and M. Braden, Crystal structure and distortion of superconducting $\text{Cu}_x\text{Bi}_2\text{Se}_3$, *Phys. Rev. Materials* **4**, 054802 (2020).
- [35] Shruti, V. K. Maurya, P. Neha, P. Srivastava, and S. Patnaik, Superconductivity by Sr intercalation in the layered topological insulator Bi_2Se_3 , *Phys. Rev. B* **92**, 020506(R) (2015).
- [36] Z. Liu, X. Yao, J. Shao, M. Zuo, L. Pi, S. Tan, C. Zhang, and Y. Zhang, Superconductivity with topological surface state in $\text{Sr}_x\text{Bi}_2\text{Se}_3$, *J. Am. Chem. Soc.* **137**, 10512 (2015).
- [37] J. Wang, F. Jiao, D. Zhang, M. Chang, L. Cai, Y. Li, C. Wang, S. Tan, Q. Jing, B. Liu, and D. Qian, Investigate the Nb doping position and its relationship with bulk topological superconductivity in $\text{Nb}_x\text{Bi}_2\text{Se}_3$ by x-ray photoelectron spectra, *J. Phys. Chem. Solids* **137**, 109208 (2020).
- [38] M. E. Kamminga, M. Batuk, J. Hadermann, and S. J. Clarke, Misfit phase $(\text{BiSe})_{1.10}\text{NbSe}_2$ as the origin of superconductivity in niobium-doped bismuth selenide, *Commun. Mater.* **1**, 82 (2020).
- [39] A. Ramires and M. Sgrist, Identifying detrimental effects for multiorbital superconductivity: Application to Sr_2RuO_4 , *Phys. Rev. B* **94**, 104501 (2016).
- [40] A. Ramires and M. Sgrist, A note on the upper critical field of Sr_2RuO_4 under strain, *J. Phys.: Conf. Ser.* **807**, 052011 (2017).
- [41] A. Ramires, D. F. Agterberg, and M. Sgrist, Tailoring T_c by symmetry principles: The concept of superconducting fitness, *Phys. Rev. B* **98**, 024501 (2018).
- [42] C. Triola, J. Cayao, and A. M. Black-Schaffer, The role of odd-frequency pairing in multiband superconductors, *Ann. Phys.* **532**, 1900298 (2020).

- [43] M. D. E. Denys and P. M. R. Brydon, Origin of the anomalous Hall effect in two-band chiral superconductors, *Phys. Rev. B* **103**, 094503 (2021).
- [44] A. Ramires, Nonunitary superconductivity in complex quantum materials, *J. Phys.: Condens. Matter* **34**, 304001 (2022).
- [45] S. Beck, A. Hampel, M. Zingl, C. Timm, and A. Ramires, Effects of strain in multiorbital superconductors: The case of Sr_2RuO_4 , *Phys. Rev. Research* **4**, 023060 (2022).
- [46] A. Ramires, Nodal gaps from local interactions in Sr_2RuO_4 , *J. Phys.: Conf. Ser.* **2164**, 012002 (2022).
- [47] S. Kanasugi and Y. Yanase, Anapole superconductivity from \mathcal{PT} -symmetric mixed-parity interband pairing, *Commun. Phys.* **5**, 39 (2022).
- [48] P. M. R. Brydon, D. F. Agterberg, H. Menke, and C. Timm, Bogoliubov Fermi surfaces: General theory, magnetic order, and topology, *Phys. Rev. B* **98**, 224509 (2018).
- [49] V. P. Mineev and K. Samokhin, *Introduction to Unconventional Superconductivity* (Gordon and Breach, 1999).
- [50] K. Maki, Gapless superconductivity, in *Superconductivity* (Routledge, 2018), pp. 1035–1105.